Title

Reversible Interlayer Sliding and Conductivity Changes in Adaptive Tetrathiafulvalene-Based Covalent Organic Frameworks

Journal

ACS Applied Materials & Interfaces, 12(16)

ISSN

1944-8244

Authors

Cai, Songliang

Sun, Bing

Li, Xinle

et al.

Publication Date

2020-04-22

DOI

10.1021/acsami.0c03280

Peer reviewed

ACS APPLIED MATERIALS & INTERFACES

www.acsami.org Research Article

Reversible Interlayer Sliding and Conductivity Changes in Adaptive Tetrathiafulvalene-Based Covalent Organic Frameworks

Songliang Cai,[¶] Bing Sun,[¶] Xinle Li, Yilun Yan, Amparo Navarro, Andrés Garzón-Ruiz, Haiyan Mao, Ruchira Chatterjee, Junko Yano, Chenhui Zhu, Jeffrey A. Reimer, Shengrun Zheng, Jun Fan, Weiguang Zhang,* and Yi Liu*

Cite This: https://dx.doi.org/10.1021/acsami.0c03280 Read Online

ACCESS | Metrics & More | Article Recommendations | Supporting Information

ABSTRACT: Ordered interlayer stacking is intrinsic in two-dimensional covalent organic frameworks (2D COFs) and has strong implications on COF's optoelectronic properties. Reversible interlayer sliding, corresponding to shearing of 2D layers along their basal plane, is an appealing dynamic control of both structures and properties, yet it remains unexplored in the 2D COF field. Herein, we demonstrate that the reversible interlayer sliding can be realized in an imine-linked tetrathiafulvalene (TTF)-based COF **TTF-DMTA**. The solvent treatment induces crystalline phase changes between the proposed staircase-like ***sql*** net structure and a slightly slipped eclipsed ***sql*** net structure. The solvation-induced crystallinity changes correlate well with reversible spectroscopic and electrical conductivity changes as demonstrated in oriented COF thin films. In contrast, no reversible switching is observed in a related **TTF-TA** COF, which differs from **TTF-DMTA** in terms of the absence of methoxy groups on the phenylene linkers. This work represents the first 2D COF example of which eclipsed and staircase-like aggregated states are interchangeably accessed via interlayer sliding, an uncharted structural feature that may enable applications such as chemiresistive sensors.

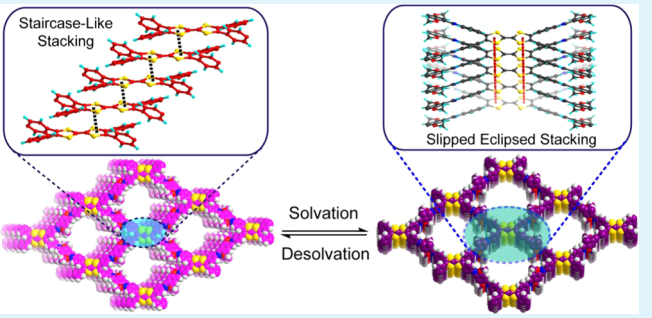

KEYWORDS: *conductivity switching, covalent organic frameworks, interlayer sliding, reversible phase transformation, solvent responsive, tetrathiafulvalene*

INTRODUCTION

Two-dimensional covalent organic framework (2D COF) is a class of synthetic layered organic materials with a periodic arrangement of repeating units, typically rigid conjugated ring systems, within a 2D layer, which are further stacked in the third dimension with a crystallographic order.[1−7] The in-plane order is conserved by strong covalent bonds, while the out-of-plane order relies on weak noncovalent interlayer interactions such as $\pi-\pi$ stacking interactions.[8,9] Crystalline framework materials can undergo lattice contraction and extension without collapsing the crystal framework when exposed to environmental stimuli, as demonstrated in metal−organic frameworks (MOFs).[10−12] Only until recently have such phenomena been demonstrated in solvent-responsive three-dimensional (3D) COFs,[13−15] while 2D COFs rarely undergo phase changes without losing crystallinity.[16] Lattice deformation was noted in a recent 2D COF example;[17] however, the contraction and expansion are confined within the 2D plane, with little information about the crystalline order on the layer stacking direction. Since interlayer stacking significantly impacts the electronic, optical, and mechanical properties of layered materials,[18] as exemplified by graphene[19] and transition-metal dichalcogenides (TMDs),[20] it is important to achieve control of the stacking order, and more ideal if reversible layer sliding and realignment can be realized, which is relevant for applications as sensors[21,22] and responsive materials.[23]

The interlayer stacking modes in 2D COFs are commonly modeled against two boundary scenarios where adjacent layers are either fully eclipsed or staggered, which are best described as close approximations, as slight offset has been proposed and supported by theoretical calculations.[9] Recent studies have revealed examples of intermediate interlayer stacking modes such as staircase[24−26] and serrated stacking.[27] Although the interlayer interactions are relatively weak and thus translational freedom is expected to facilitate layer shearing along the basal plane, no interchange between these different stacking modes has been disclosed in 2D COFs. In fact, the majority of the

Received: February 24, 2020
Accepted: March 26, 2020
Published: March 26, 2020

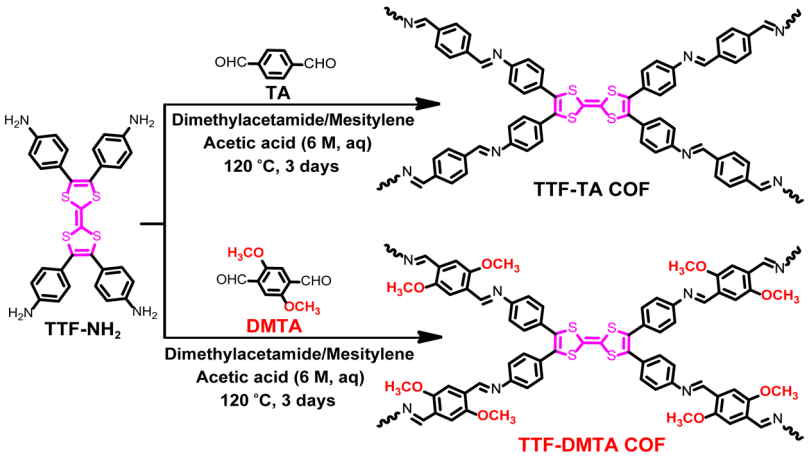

Figure 1. Syntheses of TTF-based COFs **TTF-TA** and **TTF-DMTA**.

known 2D COFs showcase the stability of their crystalline phase, implying that the interlayer interactions are rather strong such that layer sliding is circumvented. Few exceptions are noted where interlayer interactions are weak enough such that solvent treatment disrupts the crystallographic order along the stacking direction, resulting in few-layer aggregates with decreased crystallinity.[16,28−30] The question thus remains as to whether reversible layer sliding can be realized in polymorphic 2D COFs, which necessitates structural variations to fine-tune interlayer stacking interactions. Herein, we report two tetrathiafulvalene (TTF)-based imine COFs, **TTF-TA** and **TTF-DMTA**, constructed by reacting a tetraaniline-appended TTF (**TTF-NH$_2$**) with terephthalaldehyde (**TA**) and dimethoxy terephthalaldehyde (**DMTA**), respectively. The two COFs display contrasting packing structures and responses to solvent treatment. **TTF-TA** shows decreased crystallinity when exposed to polar solvents such as ethanol (EtOH), while **TTF-DMTA** undergoes a crystalline phase change upon solvent exposure, corresponding to the synchronized sliding of the 2D layers. The solvent-induced phase is transient and reverts to the original state upon desolvation. The successful realization of reversible interlayer stacking sets the stage to investigate its impact on charge transport properties in 2D COFs. Reversible changes in conductivity were observed in solvent-exposed **TTF-DMTA** COF thin films, contrasting to irreversible conductivity change in the case of **TTF-TA**, which correlates well with their crystallinity switching behavior.

RESULTS AND DISCUSSION

Material Synthesis and Characterization. TTF-based COF was previously synthesized by us[31] and several other groups[32,33] from the reaction between tetra-formylbenzene-derived TTF and 1,4-phenylenediamine. While this COF showed appealing electrical properties, further study was hampered by the nontrivial synthesis of the TTF tetraaldehyde precursor, which required tedious and lossy purification from partially arylated byproducts. In the revised COF design, we employed tetraaniline-derived TTF (**TTF-NH$_2$**), which could be obtained in high purity following routine procedures (see the Supporting Information for details). The syntheses of **TTF-TA** and **TTF-DMTA** COFs were attempted by reacting **TTF-NH$_2$** with **TA** or **DMTA** under various solvothermal conditions (Figure 1). After optimization, **TTF-TA** and **TTF-DMTA** COFs could be readily obtained by reacting the precursors at 120 °C for 3 days in a mixture of acetic acid (6 M) and dimethylacetamide/mesitylene (see Figures S1−S4).

Both COF structures were well characterized by a variety of techniques, including Fourier transform infrared (FT-IR) and ^{13}C cross-polarization magic-angle spinning (CP-MAS) solid-state NMR spectroscopies. A comparison of the FT-IR spectra of the COFs against those of the starting materials (Figures S5 and S6) revealed the appearance of the characteristic imine C═N stretching vibrations at ∼1620 cm^{-1}, together with the greatly diminished intensity of the aldehyde C═O and amine N−H stretching frequencies, suggesting the effective Schiff-base reactions. The imine bond formation also corroborated with the peaks at 162.5 and 154.2 ppm in the respective ^{13}C CP-MAS NMR spectra of **TTF-TA** and **TTF-DMTA** (Figures S7 and S8). Thermogravimetric analysis (TGA) of **TTF-TA** and **TTF-DMTA** showed no appreciable weight loss at temperatures below 380 and 350 °C, respectively, indicating the good thermal stability of these COFs (Figure S9). Scanning electron microscopy (SEM) images revealed that **TTF-TA** COF had a morphology as well-defined microcrystals (Figure S10), while the **TTF-DMTA** COF appeared as aggregates of nanorods (Figure S11). The surface area and porosity of the **TTF-TA** and **TTF-DMTA** COFs were evaluated by nitrogen adsorption−desorption measurements conducted at 77 K on samples activated by N_2 flushing. As depicted in Figures S12 and S13, both COFs displayed a type I adsorption isotherm, implying that they were typical microporous materials. The Brunauer−Emmett−Teller (BET) specific surface areas were determined to be 510 m^2 g^{-1} for **TTF-TA** and 837 m^2 g^{-1} for **TTF-DMTA**, while their total pore volumes based on a single point measurement (P/P_0 = 0.95) were calculated to be 0.35 and 0.47 cm^3 g^{-1}, respectively. The pore widths of **TTF-TA** and **TTF-DMTA** were determined to be 1.8 and 1.6 nm, respectively (Figures S14 and S15) based on simulations using Quenched solid density functional theory (QSDFT), which matched very well with the predicted values of **TTF-TA** (1.9 nm) and **TTF-DMTA** (1.7 nm).

Crystallinity Studies. The powder X-ray diffraction (PXRD) pattern of **TTF-TA** (Figure 2) exhibited a strong diffraction peak at 4.3° and two weak peaks centered at 6.9 and 8.7°, assignable to the reflections from the (110), (130), and (220) facets, respectively. It has been demonstrated that the combination of a tetradentate building block with a linear

https://dx.doi.org/10.1021/acsami.0c03280
ACS Appl. Mater. Interfaces XXXX, XXX, XXX−XXX

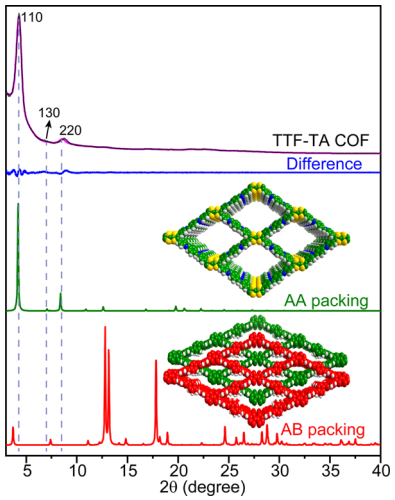

Figure 2. PXRD patterns and simulated structures of the **TTF-TA** COF. Experimental PXRD pattern of **TTF-TA** (black), Pawley refined PXRD pattern of **TTF-TA** (pink), and the difference plot of the two PXRD patterns (blue). PXRD patterns of simulated SP ***sql*** net with *s*-AA stacking (green) and AB stacking (red), and their corresponding simulated structures.

ditopic linker may produce three potential 2D layered structures with different topologies, including dual-pore (DP) ***sql***, DP ***kgm***, and single-pore (SP) ***sql*** nets.[34,35] The PXRD patterns of all three plausible structures (Figure S16) were simulated with both an eclipsed (AA) and a staggered interlayer packing (AB) using *Materials Studio* software,[36] from which the AA stacked SP ***sql*** net with a *C*2/*m* space group gave the best match with the experimental data. Pawley refinement based on this structure yielded a PXRD pattern that was consistent with the experimental pattern, affording refined unit cell parameters of a = 24.93 Å, b = 44.36 Å, c = 4.55 Å, α = γ = 90° and β = 104.86° with R_{wp} and R_p of 2.84 and 2.07%, respectively. The deviation of β from 90° correlates to a refined structure where the COF layers are slightly offset along the short TTF axis, as depicted in Figure 2. This slipped AA (denoted as *s*-AA) stacking is similar to these described in other COF systems such as pyrene-based COFs.[25,37]

The methoxy-bearing **TTF-DMTA** COF showed a PXRD pattern apparently different from that of **TTF-TA** (Figure 3). Simulations excluded the formation of DP ***sql*** and DP ***kgm*** nets due to the obvious mismatch (Figure S17). On the other hand, the pattern exhibited fair similarity to that of **TTF-TA** but with notable differences, such as the appearance of a shoulder to the 110 reflection and splitting of the 220 reflection, which was indicative of a decreased symmetry of the unit cell. Increasing the offset between adjacent layers in ***sql*** net by displacing the layers along the long TTF axis results in a lower symmetry. Simulation based on this staircase-like ***sql*** net structure matched well with the experimental pattern (Figure 3a,c). The diffraction peaks at 4.5, 5.1, 5.6, and 9.2° were attributed to the (110), ($1\bar{1}0$), (020), and (220) facets, respectively. Further Pawley refinement based on the proposed 2D staircase ***sql*** net using a P1 space group gave the following unit cell parameters: a = 24.34 Å, b = 44.82 Å, c = 5.36 Å, α = 134.44°, β = 104.86°, γ = 72.11°, with agreement factors of R_{wp} and R_p of 2.36 and 1.70%, respectively. Compared to the *s*-AA stacking model for **TTF-TA**, the layer stacking in this staircase-like model for **TTF-DMTA** requires displacement along both

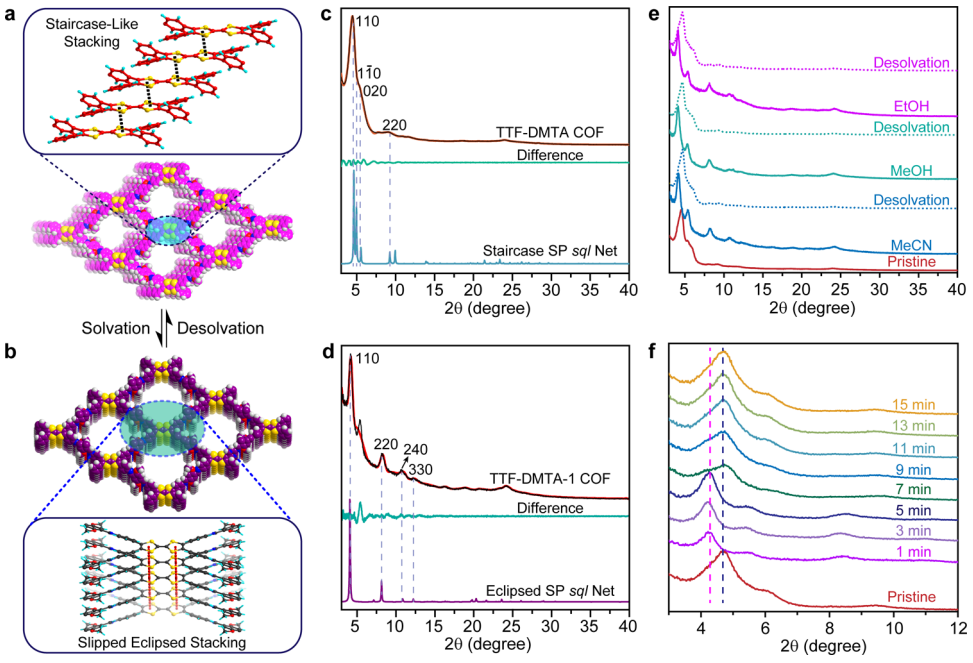

Figure 3. Reversible crystal-to-crystal phase transformation between **TTF-DMTA** and **TTF-DMTA-1** and the corresponding PXRD patterns. (a) Packing structure of the staircase SP ***sql*** type **TTF-DMTA**. The blowout shows the staircase-like interlayer stacking of the TTF units. (b) Packing structure of the *s*-AA ***sql*** type **TTF-DMTA-1** COF. The blowout shows the slipped eclipsed interlayer stacking of the TTF units. (c) PXRD patterns of the **TTF-DMTA** COF: experimental (black), Pawley refined (red), their difference (green), and simulated staircase SP ***sql*** net (pale blue). (d) PXRD patterns of the solvated **TTF-DMTA-1** COF: experimental (black), Pawley refined (red), their difference (green), and simulated *s*-AA ***sql*** net (purple). (e) PXRD pattern changes of **TTF-DMTA** toward different solvents, showing reversible crystal-to-crystal structural transformation between **TTF-DMTA** and **TTF-DMTA-1**. (f) Time-dependent PXRD pattern changes of **TTF-DMTA** to EtOH, showing the dynamic structural transformation between **TTF-DMTA** and **TTF-DMTA-1**.

https://dx.doi.org/10.1021/acsami.0c03280
ACS Appl. Mater. Interfaces XXXX, XXX, XXX−XXX

the short and long axes of the TTF unit. The symmetry reduction of the unit cell and the PXRD pattern induced by such s staircase-like interlayer stacking is similar to that of a recently reported *J*-aggregated porphyrin COF.[24]

Interestingly, the **TTF-DMTA** COF underwent reversible crystal structural transformation upon treatment with various solvents. As illustrated in Figure 3e, when immersing the COF powder in solvents such as MeCN, MeOH, and EtOH, the PXRD pattern of solvated **TTF-DMTA** changed significantly to a new and more symmetric phase (denoted as **TTF-DMTA-1**). A time-dependent study of the PXRD changes of **TTF-DMTA** upon EtOH treatment revealed that **TTF-DMTA** was converted to **TTF-DMTA-1** within the data collection period (~1 min) (Figure 3f). When the solvated sample was left in the air, its PXRD pattern reverted to the asymmetric one within a few minutes, corroborating with the evaporation of the adsorbed solvent. Such solvent-induced reversible changes were tested by sequential exposure to MeCN, MeOH, and EtOH (Figure 3e) or repeated three times using EtOH as the solvent (Figure S18), with no apparent loss of crystallinity, confirming the reversibility and cycling stability of the phase changes. In contrast, treating **TTF-TA** with EtOH solvent led to irreversible crystallinity loss, together with the shift and broadening of the (100) peak, which did not recover after prolonged solvent evacuation (Figure S19).

Analysis of the PXRD pattern of the solvated **TTF-DMTA-1** COF revealed great resemblance to that of **TTF-TA** COF with a *s*-AA-stacked SP ***sql*** net structure, as was further supported by simulation (Figure 3b,d). The peaks at 2θ = 4.1, 8.2, 10.7, and 12.2° could be assigned to the (110), (220), (240), and (330) facets, respectively. Pawley refinement based on a *s*-AA-stacked SP ***sql*** net showed good agreement with the following unit cell parameters: a = 25.16 Å, b = 42.30 Å, c = 4.50 Å, $\alpha = \gamma$ = 90°, β = 95.05° (R_{wp} = 4.17%, R_p = 2.81%). The reflection at ~5°, which is missing in the simulated XRD of **TTF-DMTA-1**, might suggest the coexistence of some residue phases from **TTF-DMTA**, while other unknown phases coexisting in the system cannot be excluded. The reversible crystalline phase change in **TTF-DMTA** suggested in-plane lattice deformations due to solvent adsorption/desorption, commensurate with synchronized sliding of the 2D layers such that the crystallographic order on the stacking direction can be preserved. In contrast, the irreversible phase change in solvent-treated **TTF-TA** suggested that lattice contractions significantly disrupted the interlayer stacking and rendered the loss of crystallinity. The weakened interlayer stacking was supported by atomic force microscopy (AFM) studies of the **TTF-TA** samples prepared after sonication in EtOH, which revealed micron-sized sheetlike structures. The thickness was only 3.3 nm, corresponding to a few COF layers (Figure S20). In contrast, similarly treated **TTF-DMTA** COF samples showed very different morphologies with a nonuniform thickness (Figure S21).

Theoretical Modeling. Density functional theory (DFT) calculations were carried out to provide more insight into the solvent-induced crystalline phase change observed in **TTF-DMTA**. Before modeling the periodic structures of the COFs in the presence and absence of solvent, it is prudent to investigate how the solvent molecules are localized in the framework. The evolution of the Raman spectrum of **TTF-DMTA** upon treatment with EtOH provided good experimental clues. The intensities of the bands observed at 1150 cm^{-1} and, more pronouncedly, at 1669 cm^{-1} decreased in the presence of the solvent and rose again when the solvent was evaporated (see Figure S22a). The computed Raman spectrum of a monomeric TTF unit (see Figures S22b, S23, and S24) indicated that bands at 1669 and 1150 cm^{-1} correspond to C═N stretching vibrations and rocking modes in the dimethoxyphenyl rings, respectively. The simulation suggested that both MeOH and MeCN solvent molecules can establish hydrogen bonding with the nearby imine and methoxy groups, forming a six-membered pseudo-ring and stabilizing the molecular structure (see Figure S24). The presence of solvent molecules at this position leads to significant changes in the molecular structure, especially involving the torsions between dimethoxyphenyl rings and TTF core, and is consistent with the loss of intensity of the bands at 1150 and 1669 cm^{-1} (see Figures S23 and S24 and Table S1 for more details).

Based on the solvent−molecule interaction model, **TTF-TA**, **TTF-DMTA**, and **TTF-DMTA-1** periodic structures were modeled at the DFT level, employing the above-mentioned simulated crystal structures as the starting point and incorporating the solvent molecules (using MeOH for simplicity) at the indicated positions in the case of **TTF-DMTA-1** (see the Supporting Information for computational details). In agreement with experimental observations, DFT calculations yielded slipped eclipsed structures for both **TTF-DMTA-1** and **TTF-TA** crystals (Figures 4 and S25), and staircase packing for **TTF-DMTA** with an interlayer $\pi-\pi$

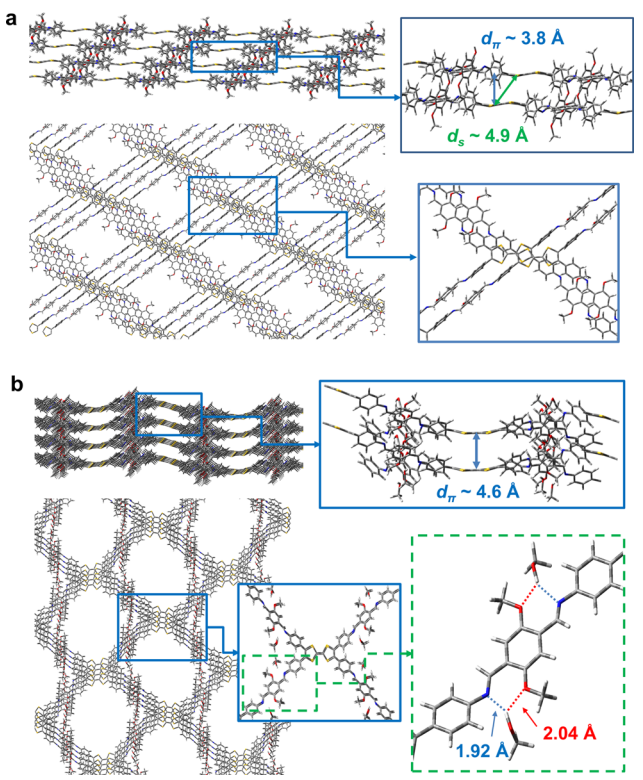

Figure 4. Calculated crystal packing structures for **TTF-DMTA** and **TTF-DMTA-1** using periodic boundary conditions at the HSE06/3-21G* level of theory. (a) Crystal packing structure for **TTF-DMTA** (in the absence of methanol). (b) Crystal packing structure for **TTF-DMTA-1** (in the presence of methanol). Zoomed images of different stacking arrangements of **TTF-DMTA** and the π-stacking distance between TTF cores (d_π), the displacement distance between TTF cores (d_s), and the localization of the solvent molecules forming a six-membered pseudo-ring with amine and methoxy groups.

https://dx.doi.org/10.1021/acsami.0c03280
ACS Appl. Mater. Interfaces XXXX, XXX, XXX−XXX

distance of ~3.8 Å. In general, larger dihedral angles between conjugated rings were computed for **TTF-DMTA** than for **TTF-DMTA-1**, but the interlayer $\pi-\pi$ distance in the solvated **TTF-DMTA-1** COF shows an increase of about 0.8 Å with respect to the staircase-stacked **TTF-DMTA** (Figure 4).

Oriented COF Thin Film Growth, Optical Characterization, and Modeling. COF thin films of both **TTF-DMTA** and **TTF-TA** with thicknesses of around 100 nm were successfully grown onto modified silicon or transparent ITO-coated glass substrates using slightly different conditions from the bulk powder synthesis. Grazing incidence wide-angle X-ray scattering (GIWAXS) experiments were carried out to verify the crystallinity of these thin films. In-plane Bragg diffraction rods, together with a strong out-of-plane $\pi-\pi$ stacking peak, were observed for both COF thin films grown on silicon (Figures 5a,b and S26) or ITO-glass substrates (see Figure S27), indicating the preferential orientation of COF crystallites with the 2D layers lying parallel to the substrate. In-plane linecuts show diffraction patterns that are identical to those of the powder samples, further confirming the crystallinity of these thin films.

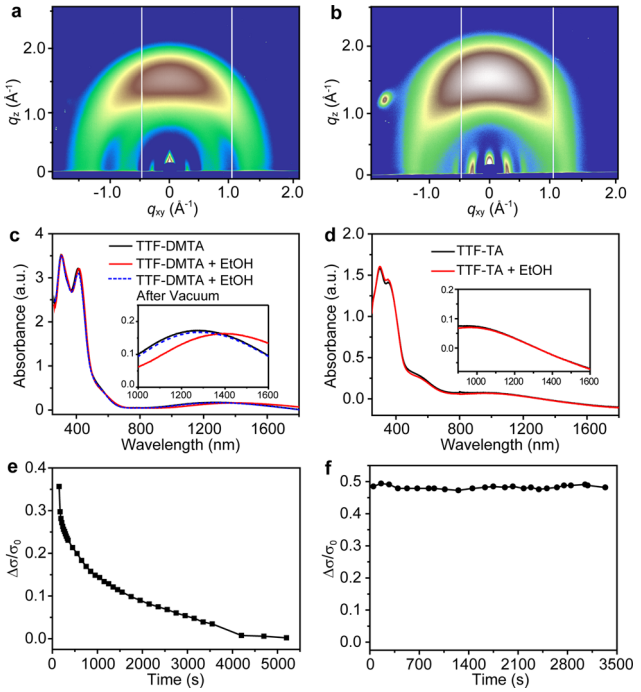

Figure 5. GIWAXS, UV−vis−NIR spectra, and conductivity measurements of **TTF-DMTA** and **TTF-TA**. (a) GIWAXS pattern of the **TTF-DMTA** COF thin film grown on a silicon substrate. (b) GIWAXS pattern of the **TTF-TA** COF thin film grown on a silicon substrate. (c) UV−vis−NIR spectra of the **TTF-DMTA** COF thin film before and after treating with EtOH. Insets are the zoomed-in images of the NIR region showing reversible absorption changes. (d) UV−vis−NIR spectra of the **TTF-TA** COF before and after treating with EtOH. (e) Representative plot of conductivity change against time for EtOH-treated thin film of **TTF-DMTA**. (f) Representative plot of conductivity change against time for EtOH-treated thin films of **TTF-TA**.

Ethanol treatment of **TTF-DMTA** induced visual color changes from brown to blackish brown (inset in Figure S28); in contrast, no color change was observed for the similarly treated **TTF-TA**. Such visual changes were consistent with the UV−vis−near IR (NIR) responses of COFs in both the solid form (Figure S28) and the thin film form (Figure 5c). The UV−vis−NIR spectrum of a **TTF-DMTA** thin film grown onto a transparent ITO-coated glass substrate exhibited two sharp peaks centered at 305 and 411 nm and two low-intensity peaks at ~550 and 1280 nm. The broad peak in the NIR region was also observed in the spectrum of the **TTF-DMTA** solid (~1000 nm, Figure S28), which is characteristic of the $TTF^{\bullet+}$ radical cation species and agrees with the theoretical simulations of the macrocyclic tetrameric TTF unit cell (see details in Table S2). The spectral feature is also consistent with that of the previously reported TTF-based COF, attributable to partial oxidation of TTF during the synthesis.[31] When treated with EtOH, a slight but discernible red shift of all the absorption peaks was observed with a broad radical cation absorption being the most obviously shifted. Such solvatochromic changes are concurrent with the phase change to the solvated **TTF-DMTA-1**. Evacuation of the solvent by vacuum resulted in the full recovery of the spectrum of **TTF-DMTA**. The spectroscopic behavior was in contrast to that of the **TTF-TA** COF thin films, which displayed no peak shift upon solvent treatment (Figure 5d).

The solvent effect on the absorption spectrum and the presence of radical cations were also simulated by time-dependent (TD)-DFT calculations on oligomeric subunits (monomers, dimers, and macrocyclic tetramers, see Figure S29) extracted from the modeled COF crystal structures. As experimentally observed, the calculated absorption spectra for oligomers from **TTF-DMTA-1** and **TTF-TA** are red-shifted with respect to that from **TTF-DMTA** (see Figure S30a), attributable to the more planar structure and, accordingly, the more efficient conjugation. In addition, the band experimentally observed at 411 nm corresponds to an intramolecular charge transfer from the TTF cores (where the highest occupied molecular orbitals (HOMOs) are localized) to DMTA (or TA) linkers (where the lowest unoccupied molecular orbitals (LUMOs) are localized) (see Figure S31). In the monocationic form, a new electronic transition (β-HOMO-$n\rightarrow\beta$-SOMO, where $n \geq 0$) around 1000 nm in the NIR region appears, confirming the presence of radical cation $TTF^{\bullet+}$ species in the COF (see Figure S30b).

The absorption features and the radical characteristics corroborate well with electron spin resonance (ESR) spectroscopic studies. As shown in Figure S33, both **TTF-TA** and **TTF-DMTA** powder showed a resonance in the X-band with a g value of 2.037, corresponding to the presence of doped TTF radical cations and is consistent with the absorption spectrum. The addition of a drop of EtOH (40 μL) into the solid sample incurs a slight decrease of the EPR intensity for both COFs, suggesting a slight quenching effect of the radical species.

Electrical Characterization of COF Thin Films and Modeling. The reversible interlayer sliding within **TTF-DMTA** prompted us to investigate its impact on electrical conductivity. Thin films of **TTF-DMTA** with a thickness of ~100 nm were grown on APTES-modified silicon substrates, onto which pairs of gold top electrodes were deposited by evaporation. Two-contact measurement on the solvent-free COF thin film gave a linear current−voltage ($I-V$) response (Figure S34) and a corresponding conductivity (σ) of 1.3×10^{-4} S/m. Treating the **TTF-DMTA** thin film with EtOH resulted in an increase of the conductivity to 1.8×10^{-4} S/m, which was transient and decayed over time back to the same value as that of the solvent-free COF (Figure 5e). Similar $I-V$

https://dx.doi.org/10.1021/acsami.0c03280
ACS Appl. Mater. Interfaces XXXX, XXX, XXX−XXX

responses were observed in three independent devices fabricated on separate substrates, with initial σ in the range of 1.5×10^{-4} to 1.7×10^{-4} S/m and $\Delta\sigma/\sigma$ between 0.58 and 0.66 (Figure S35). In comparison, when the COF thin film was treated with a nonpolar solvent such as pentane, only a slight change in conductivity (~7%) was observed (Figure S36a). Correspondingly, no solvent-induced changes were observed in the PXRD spectra of **TTF-DMTA** powder (Figure S36b). This insignificant conductivity response is in contrast to the EtOH-induced conductivity changes and corroborates well with the lack of phase changes in pentane-treated **TTF-DMTA** COFs. In the case of **TTF-TA**, its thin film also experienced an increase in conductivity upon exposure to EtOH (Figure S37); however, it remained constant after the solvent was evaporated (Figure 5f). The different conductivity responses corroborate well with the solvent-induced crystallinity changes observed in **TTF-DMTA** and **TTF-TA** COFs, respectively, which suggest their potential application as chemiresistive sensors for volatile organic compounds. To the best of our knowledge, while chemiresistive sensing has been demonstrated in MOF and COF materials,[38−42] **TTF-DMTA** represents the first COF example that displays reversible guest-induced interlayer packing and conductivity changes.

At the molecular level, the conductivity switching exhibited in **TTF-DMTA** COF was investigated through the Marcus theory in which the charge motion is generally described by a hopping mechanism that is particularly efficient along the $\pi-\pi$ stacking direction.[43−45] The charge-transfer integral (t) and the reorganization energy (λ) are the two key parameters that must be maximized and minimized, respectively, to increase the charge transfer rate constant (k_{CT}). The evolution of the values of λ and t with the size of diverse oligomeric subunits of **TTF-TA**, **TTF-DMTA**, and **TTF-DMTA-1** (from the monomer to the macrocyclic tetramer) was evaluated at DFT level (see Figure S32 and Table S3). Two main results can be extracted from calculations: first, the least planar COF, **TTF-DMTA**, yields the highest reorganization energies; second, the eclipsed structures of **TTF-TA**, and, particularly, **TTF-DMTA-1** show, in general, higher t values than **TTF-DMTA** despite its larger π-stacking distance. Accordingly, the addition of solvent molecules to **TTF-DMTA** increases the value of k_{CT} for both electrons and holes, resulting in improved conducting properties, in agreement with our experimental observations.

CONCLUSIONS

Our studies on two TTF-containing COFs with slightly different linker structures have demonstrated that subtle structural changes lead to quite contrasting polymorphic behavior that has been rarely observed in COFs. Simulated structures based on the PXRD studies suggest that while **TTF-TA** adopts a slipped eclipsed (*s*-AA) structure, which loses crystallinity upon treatment with polar solvents, the methoxy-containing **TTF-DMTA** assumes a lower-symmetry, staircase-like structure, which reversibly switches to a *s*-AA structure in response to solvent treatment. It is worth noting that these are structural models derived from fitting the PXRD pattern with simulated structures. The exact structure might have slight deviations from the proposed models, the assignment of which is unfeasible, given only a handful of clearly identifiable reflections. Accompanying the solvent-stimulated interlayer sliding, consistent spectroscopic and electrical conductivity changes were observed. This work represents the first COF example in which different packing states are interchangeably accessed in ordered framework structures, which subsequently influence the charge-transport properties. Postsynthetic processing-induced change of packing and charge transport properties has been more commonly observed in small-molecule organic semiconductors and conjugated polymers but not in COF materials. This finding thus adds a new dimension of dynamic control of the conceptually rigid organic frameworks for fine-tuning the physicochemical properties.

ASSOCIATED CONTENT

Supporting Information

The Supporting Information is available free of charge at https://pubs.acs.org/doi/10.1021/acsami.0c03280.

Complete synthetic procedure, IR spectra, solid-state ^{13}C NMR spectra, SEM, TGA trace, conductivity measurement, UV−vis−NIR spectra, AFM topographic images, Raman spectra, EPR spectra, GIWAXS data, MALDI-MS, PXRD analysis, and coordinates of crystal structure models (PDF)

AUTHOR INFORMATION

Corresponding Authors

Weiguang Zhang − *School of Chemistry, South China Normal University, Guangzhou 510006, P. R. China;* orcid.org/0000-0002-3697-2990; Email: wgzhang@scnu.edu.cn

Yi Liu − *The Molecular Foundry, Lawrence Berkeley National Laboratory, Berkeley, California 94720, United States;* orcid.org/0000-0002-3954-6102; Email: yliu@lbl.gov

Authors

Songliang Cai − *School of Chemistry, South China Normal University, Guangzhou 510006, P. R. China; The Molecular Foundry, Lawrence Berkeley National Laboratory, Berkeley, California 94720, United States;* orcid.org/0000-0002-5399-9036

Bing Sun − *The Molecular Foundry, Lawrence Berkeley National Laboratory, Berkeley, California 94720, United States; School of Science, China University of Geosciences (Beijing), Beijing 100083, P. R. China;* orcid.org/0000-0001-5917-3094

Xinle Li − *The Molecular Foundry, Lawrence Berkeley National Laboratory, Berkeley, California 94720, United States*

Yilun Yan − *School of Chemistry, South China Normal University, Guangzhou 510006, P. R. China*

Amparo Navarro − *Department of Physical and Analytical Chemistry, Faculty of Experimental Sciences, Universidad de Jaén, Jaén 23071, Spain;* orcid.org/0000-0001-9620-6668

Andrés Garzón-Ruiz − *Department of Physical Chemistry, Faculty of Pharmacy, Universidad de Castilla-La Mancha, Albacete 02071, Spain;* orcid.org/0000-0002-0077-4562

Haiyan Mao − *Department of Chemical and Biomolecular Engineering, University of California, Berkeley, California 94720, United States; College of Materials Science and Engineering, Nanjing Forestry University, Nanjing 210037, P. R. China*

Ruchira Chatterjee − *Molecular Biophysics and Integrated Bioimaging Division, Lawrence Berkeley National Laboratory, Berkeley, California 94720, United States*

Junko Yano − *Molecular Biophysics and Integrated Bioimaging Division, Lawrence Berkeley National Laboratory, Berkeley, California 94720, United States;* orcid.org/0000-0001-6308-9071

https://dx.doi.org/10.1021/acsami.0c03280
ACS Appl. Mater. Interfaces XXXX, XXX, XXX−XXX

Chenhui Zhu − *Advanced Light Source, Lawrence Berkeley National Laboratory, Berkeley, California 94720, United States*
Jeffrey A. Reimer − *Department of Chemical and Biomolecular Engineering, University of California, Berkeley, California 94720, United States;* orcid.org/0000-0002-4191-3725
Shengrun Zheng − *School of Chemistry, South China Normal University, Guangzhou 510006, P. R. China*
Jun Fan − *School of Chemistry, South China Normal University, Guangzhou 510006, P. R. China;* orcid.org/0000-0003-2986-8551

Complete contact information is available at: https://pubs.acs.org/10.1021/acsami.0c03280

Author Contributions

[¶]S.C. and B.S. contributed equally to this work.

Notes

The authors declare no competing financial interest.

■ ACKNOWLEDGMENTS

This work was performed as a user project at the Molecular Foundry, Lawrence Berkeley National Laboratory, and GIWAXS data were collected at BL7.3.3 at Advanced Light Source, both supported by the Office of Science, Office of Basic Energy Sciences, U.S. Department of Energy under Contract No. DE-AC02-05CH11231. We gratefully acknowledge the financial support from the National Natural Science Foundation of P. R. China (Grant Nos. 21603076, 21571070, and 21802128), and the Natural Science Foundation of Guangdong Province (Grant No. 2018A030313193). A.N. and A.G.-R. thank Centro de Servicios de Informática y Redes de Comunicaciones (CSIRC) (Universidad de Granada, Spain) for providing the computing time, Consejeria de Economía y Conocimiento, Junta de Andalucía (FQM-337), Acción 1_Plan 2017-18 (Universidad de Jaén, Spain) and Ministerio de Economía y Competitividad (Spain) (project CTQ2017-84561-P). S.C. is grateful to South China Normal University for providing a scholarship for his stay at Lawrence Berkeley National Laboratory. B.S. acknowledges the support of the China Scholarship Council (CSC). We also thank Dr. Hassan Celik, Dr. Nanette Jarenwattananon, and the SSNMR facility from the Department of Chemical and Biomolecular Engineering, University of California, Berkeley for assistance with solid-state NMR measurements.

■ REFERENCES

(1) Ding, S.-Y.; Wang, W. Covalent Organic Frameworks (COFs): From Design to Applications. *Chem. Soc. Rev.* **2013**, *42*, 548−568.
(2) Cai, S.-L.; Zhang, W.-G.; Zuckermann, R. N.; Li, Z.-T.; Zhao, X.; Liu, Y. The Organic Flatland—Recent Advances in Synthetic 2D Organic Layers. *Adv. Mater.* **2015**, *27*, 5762−5770.
(3) Diercks, C. S.; Yaghi, O. M. The Atom, the Molecule, and the Covalent Organic Framework. *Science* **2017**, *355*, No. eaal1585.
(4) Feng, X.; Schlüter, A. D. Towards Macroscopic Crystalline 2D Polymers. *Angew. Chem., Int. Ed.* **2018**, *57*, 13748−13763.
(5) Yu, F.; Liu, W.; Li, B.; Tian, D.; Zuo, J. L.; Zhang, Q. Phtostimulus-Responsive Large-Area Two-Dimensional Covalent Organic Framework Films. *Angew. Chem., Int. Ed.* **2019**, *58*, 16101−16104.
(6) Zhang, X.; Chen, Z.; Zhang, Q. Recent Progress in Two-Dimensional COFs for Energy-Related Applications. *J. Mater. Chem. A* **2017**, *5*, 14463−14479.
(7) Yao, C. J.; Wu, Z.; Xie, J.; Yu, F.; Guo, W.; Xu, Z. J.; Li, D. S.; Zhang, S.; Zhang, Q. Two-Dimensional (2D) Covalent Organic Framework as Efficient Cathode for Binder-free Lithium-Ion Battery. *ChemSusChem* **2020**, DOI: 10.1002/cssc.201903007.
(8) Evans, A. M.; Parent, L. R.; Flanders, N. C.; Bisbey, R. P.; Vitaku, E.; Kirschner, M. S.; Schaller, R. D.; Chen, L. X.; Gianneschi, N. C.; Dichtel, W. R. Seeded Growth of Single-Crystal Two-Dimensional Covalent Organic Frameworks. *Science* **2018**, *361*, 52−57.
(9) Spitler, E. L.; Koo, B. T.; Novotney, J. L.; Colson, J. W.; Uribe-Romo, F. J.; Gutierrez, G. D.; Clancy, P.; Dichtel, W. R. A 2D Covalent Organic Framework with 4.7-nm Pores and Insight into Its Interlayer Stacking. *J. Am. Chem. Soc.* **2011**, *133*, 19416−19421.
(10) Bezuidenhout, C. X.; Smith, V. J.; Esterhuysen, C.; Barbour, L. J. Solvent- and Pressure-Induced Phase Changes in Two 3D Copper Glutarate-Based Metal−Organic Frameworks via Glutarate (+gauche ⇄ −gauche) Conformational Isomerism. *J. Am. Chem. Soc.* **2017**, *139*, 5923−5929.
(11) Halder, A.; Ghoshal, D. Structure and Properties of Dynamic Metal−Organic Frameworks: A Brief Accounts of Crystalline-to-Crystalline and Crystalline-to-Amorphous Transformations. *CrystEngComm* **2018**, *20*, 1322−1345.
(12) Liu, D.; Liu, T.-F.; Chen, Y.-P.; Zou, L.; Feng, D.; Wang, K.; Zhang, Q.; Yuan, S.; Zhong, C.; Zhou, H.-C. A Reversible Crystallinity-Preserving Phase Transition in Metal−Organic Frameworks: Discovery, Mechanistic Studies, and Potential Applications. *J. Am. Chem. Soc.* **2015**, *137*, 7740−7746.
(13) Ma, Y.-X.; Li, Z.-J.; Wei, L.; Ding, S.-Y.; Zhang, Y.-B.; Wang, W. A Dynamic Three-Dimensional Covalent Organic Framework. *J. Am. Chem. Soc.* **2017**, *139*, 4995−4998.
(14) Chen, Y.; Shi, Z.-L.; Wei, L.; Zhou, B.; Tan, J.; Zhou, H.-L.; Zhang, Y.-B. Guest-Dependent Dynamics in a 3D Covalent Organic Framework. *J. Am. Chem. Soc.* **2019**, *141*, 3298−3303.
(15) Ma, T.; Kapustin, E. A.; Yin, S. X.; Liang, L.; Zhou, Z.; Niu, J.; Li, L.-H.; Wang, Y.; Su, J.; Li, J.; Wang, X.; Wang, W. D.; Wang, W.; Sun, J.; Yaghi, O. M. Single-Crystal X-ray Diffraction Structures of Covalent Organic Frameworks. *Science* **2018**, *361*, 48−52.
(16) Sick, T.; Rotter, J. M.; Reuter, S.; Kandambeth, S.; Bach, N. N.; Döblinger, M.; Merz, J.; Clark, T.; Marder, T. B.; Bein, T.; Medina, D. D. Switching on and off Interlayer Correlations and Porosity in 2D Covalent Organic Frameworks. *J. Am. Chem. Soc.* **2019**, *141*, 12570−12581.
(17) Zhao, C.; Diercks, C. S.; Zhu, C.; Hanikel, N.; Pei, X.; Yaghi, O. M. Urea-Linked Covalent Organic Frameworks. *J. Am. Chem. Soc.* **2018**, *140*, 16438−16441.
(18) Radin, M. D.; Alvarado, J.; Meng, Y. S.; Van der Ven, A. Role of Crystal Symmetry in the Reversibility of Stacking-Sequence Changes in Layered Intercalation Electrodes. *Nano Lett.* **2017**, *17*, 7789−7795.
(19) Wang, Z.-J.; Dong, J.; Cui, Y.; Eres, G.; Timpe, O.; Fu, Q.; Ding, F.; Schloegl, R.; Willinger, M.-G. Stacking Sequence and Interlayer Coupling in Few-Layer Graphene Revealed by in situ Imaging. *Nat. Commun.* **2016**, *7*, No. 13256.
(20) Li, H.; Li, Y.; Aljarb, A.; Shi, Y.; Li, L.-J. Epitaxial Growth of Two-Dimensional Layered Transition-Metal Dichalcogenides: Growth Mechanism, Controllability, and Scalability. *Chem. Rev.* **2018**, *118*, 6134−6150.
(21) Albacete, P.; López-Moreno, A.; Mena-Hernando, S.; Platero-Prats, A. E.; Pérez, E. M.; Zamora, F. Chemical Sensing of Water Contaminants by A Colloid of A Fluorescent Imine-linked Covalent Organic Framework. *Chem. Commun.* **2019**, *55*, 1382−1385.
(22) Albacete, P.; Martínez, J. I.; Li, X.; López-Moreno, A.; Mena-Hernando, Sa.; Platero-Prats, A. E.; Montoro, C.; Loh, K. P.; Pérez, E. M.; Zamora, F. Layer-Stacking-Driven Fluorescence in A Two-Dimensional Imine-Linked Covalent Organic Framework. *J. Am. Chem. Soc.* **2018**, *140*, 12922−12929.
(23) Ascherl, L.; Evans, E. W.; Hennemann, M.; Di Nuzzo, D.; Hufnagel, A. G.; Beetz, M.; Friend, R. H.; Clark, T.; Bein, T.; Auras, F. Solvatochromic Covalent Organic Frameworks. *Nat. Commun.* **2018**, *9*, No. 3802.
(24) Keller, N.; Calik, M.; Sharapa, D.; Soni, H. R.; Zehetmaier, P. M.; Rager, S.; Auras, F.; Jakowetz, A. C.; Görling, A.; Clark, T.; Bein,

T. Enforcing Extended Porphyrin J-Aggregate Stacking in Covalent Organic Frameworks. *J. Am. Chem. Soc.* **2018**, *140*, 16544−16552.
(25) Auras, F.; Ascherl, L.; Hakimioun, A. H.; Margraf, J. T.; Hanusch, F. C.; Reuter, S.; Bessinger, D.; Döblinger, M.; Hettstedt, C.; Karaghiosoff, K.; Herbert, S.; Knochel, P.; Clark, T.; Bein, T. Synchronized Offset Stacking: A Concept for Growing Large-Domain and Highly Crystalline 2D Covalent Organic Frameworks. *J. Am. Chem. Soc.* **2016**, *138*, 16703−16710.
(26) Ascherl, L.; Sick, T.; Margraf, J. T.; Lapidus, S. H.; Calik, M.; Hettstedt, C.; Karaghiosoff, K.; Döblinger, M.; Clark, T.; Chapman, K. W.; Auras, F.; Bein, T. Molecular Docking Sites Designed for the Generation of Highly Crystalline Covalent Organic Frameworks. *Nat. Chem.* **2016**, *8*, 310−316.
(27) Lukose, B.; Kuc, A.; Heine, T. The Structure of Layered Covalent-Organic Frameworks. *Chem. - Eur. J.* **2011**, *17*, 2388−2392.
(28) Bunck, D. N.; Dichtel, W. R. Bulk Synthesis of Exfoliated Two-Dimensional Polymers Using Hydrazone-Linked Covalent Organic Frameworks. *J. Am. Chem. Soc.* **2013**, *135*, 14952−14955.
(29) Wang, S.; Wang, Q.; Shao, P.; Han, Y.; Gao, X.; Ma, L.; Yuan, S.; Ma, X.; Zhou, J.; Feng, X.; Wang, B. Exfoliation of Covalent Organic Frameworks into Few-Layer Redox-Active Nanosheets as Cathode Materials for Lithium-Ion Batteries. *J. Am. Chem. Soc.* **2017**, *139*, 4258−4261.
(30) Mitra, S.; Kandambeth, S.; Biswal, B. P.; Khayum M, A.; Choudhury, C. K.; Mehta, M.; Kaur, G.; Banerjee, S.; Prabhune, A.; Verma, S.; Roy, S.; Kharul, U. K.; Banerjee, R. Self-Exfoliated Guanidinium-Based Ionic Covalent Organic Nanosheets (iCONs). *J. Am. Chem. Soc.* **2016**, *138*, 2823−2828.
(31) Cai, S.-L.; Zhang, Y.-B.; Pun, A. B.; He, B.; Yang, J.; Toma, F. M.; Sharp, I. D.; Yaghi, O. M.; Fan, J.; Zheng, S.-R.; Zhang, W.-G.; Liu, Y. Tunable Electrical Conductivity in Oriented Thin Films of Tetrathiafulvalene-Based Covalent Organic Framework. *Chem. Sci.* **2014**, *5*, 4693−4700.
(32) Jin, S.; Sakurai, T.; Kowalczyk, T.; Dalapati, S.; Xu, F.; Wei, H.; Chen, X.; Gao, J.; Seki, S.; Irle, S.; Jiang, D.-L. Two-Dimensional Tetrathiafulvalene Covalent Organic Frameworks: Towards Latticed Conductive Organic Salts. *Chem. Eur. J.* **2014**, *20*, 14608−14613.
(33) Ding, H.; Li, Y.; Hu, H.; Sun, Y.; Wang, J.; Wang, C.; Wang, C.; Zhang, G.; Wang, B.; Xu, W.; Zhang, D. A Tetrathiafulvalene-Based Electroactive Covalent Organic Framework. *Chem. - Eur. J.* **2014**, *20*, 14614−14618.
(34) Dong, W.-L.; Wang, L.; Ding, H.-m.; Zhao, L.; Wang, D.; Wang, C.; Wan, L.-J. Substrate Orientation Effect in the on-Surface Synthesis of Tetrathiafulvalene-Integrated Single-Layer Covalent Organic Frameworks. *Langmuir* **2015**, *31*, 11755−11759.
(35) Zhou, T.-Y.; Xu, S.-Q.; Wen, Q.; Pang, Z.-F.; Zhao, X. One-Step Construction of Ewo Different Kinds of Pores in A 2D Covalent Organic Framework. *J. Am. Chem. Soc.* **2014**, *136*, 15885−15888.
(36) Accelrys Software Inc. *Materials Studio 5.0: Modeling Simulation for Chemical and Material*; San Diego, CA, 2009.
(37) Keller, N.; Bessinger, D.; Reuter, S.; Calik, M.; Ascherl, L.; Hanusch, F. C.; Auras, F.; Bein, T. Oligothiophene-Bridged Conjugated Covalent Organic Frameworks. *J. Am. Chem. Soc.* **2017**, *139*, 8194−8199.
(38) Campbell, M. G.; Sheberla, D.; Liu, S. F.; Swager, T. M.; Dincă, M. Cu_3(Hexaiminotriphenylene)$_2$: An Electrically Conductive 2D Metal−Organic Framework for Chemiresistive Sensing. *Angew. Chem., Int. Ed.* **2015**, *54*, 4349−4352.
(39) Campbell, M. G.; Liu, S. F.; Swager, T. M.; Dincă, M. Chemiresistive Sensor Arrays from Conductive 2D Metal−Organic Frameworks. *J. Am. Chem. Soc.* **2015**, *137*, 13780−13783.
(40) Aubrey, M. L.; Kapelewski, M. T.; Melville, J. F.; Oktawiec, J.; Presti, D.; Gagliardi, L.; Long, J. R. Chemiresistive Detection of Gaseous Hydrocarbons and Interrogation of Charge Transport in Cu[Ni(2,3-Pyrazinedithiolate)$_2$] by Gas Adsorption. *J. Am. Chem. Soc.* **2019**, *141*, 5005−5013.
(41) Meng, Z.; Stolz, R. M.; Mirica, K. A. Two-Dimensional Chemiresistive Covalent Organic Framework with High Intrinsic Conductivity. *J. Am. Chem. Soc.* **2019**, *141*, 11929−11937.
(42) Marcus, R. A. Electron Transfer Reactions in Chemistry: Theory and Experiment. *Rev. Mod. Phys.* **1993**, *65*, No. 599.
(43) Coropceanu, V.; Cornil, J.; da Silva Filho, D. A.; Olivier, Y.; Silbey, R.; Brédas, J.-L. Charge Transport In Organic Semiconductors. *Chem. Rev.* **2007**, *107*, 926−952.
(44) Troisi, A. Charge Transport in High Mobility Molecular Semiconductors: Classical Models and New Theories. *Chem. Soc. Rev.* **2011**, *40*, 2347−2358.
(45) Wang, L.; Nan, G.; Yang, X.; Peng, Q.; Li, Q.; Shuai, Z. Computational Methods for Design of Organic Materials with High Charge Mobility. *Chem. Soc. Rev.* **2010**, *39*, 423−434.

https://dx.doi.org/10.1021/acsami.0c03280
ACS Appl. Mater. Interfaces XXXX, XXX, XXX−XXX